Gaussian Lagrangian stochastic models for multi-particle dispersion

B. L. Sawford, S. B. Pope, and P. K. Yeung

Citation: Physics of Fluids (1994-present) **25**, 055101 (2013); doi: 10.1063/1.4802037
View online: http://dx.doi.org/10.1063/1.4802037
View Table of Contents: http://scitation.aip.org/content/aip/journal/pof2/25/5?ver=pdfcov
Published by the AIP Publishing

PHYSICS OF FLUIDS **25**, 055101 (2013)

Gaussian Lagrangian stochastic models for multi-particle dispersion

B. L. Sawford,[1,a)] S. B. Pope,[2] and P. K. Yeung[3]
[1]*Department of Mechanical and Aerospace Engineering, Monash University, Wellington Road, Clayton, Victoria 3800, Australia*
[2]*Sibley School of Mechanical and Aerospace Engineering, Cornell University, Ithaca, New York 14853-7501, USA*
[3]*Schools of Aerospace Engineering, Computational Science and Engineering, and Mechanical Engineering, Georgia Institute of Technology, Atlanta, Georgia 30332, USA*

(Received 4 October 2012; accepted 11 March 2013; published online 7 May 2013)

We have extended the "well-mixed" two-particle stochastic models for 3D Gaussian turbulence to n particles, and have performed calculations for clusters of $n \leq 6$ particles. The particle joint motions are Gaussian and are constrained by pair-wise spatial correlations. This neglects non-Gaussian properties of the two-point velocity distribution and also neglects multi-point correlations. It also takes no account of intermittency. Although the models do not predict the growth of the separation of particles in the cluster satisfactorily, we find that they do give a good representation of the shape statistics for the cluster in comparison with direct numerical simulation results. We conclude that the pair-wise spatial structure of the turbulence accounts for most of the observed characteristics of the shape of multi-particle clusters in turbulence, and that non-Gaussian and multi-point features of the turbulence are of secondary importance. © *2013 AIP Publishing LLC*. [http://dx.doi.org/10.1063/1.4802037]

I. INTRODUCTION

We are concerned in this paper with Lagrangian stochastic models of turbulent transport and mixing which, at some level, treat the trajectories of fluid elements as continuous Markov processes. Most commonly, the Lagrangian velocity, the velocity following a particle along its trajectory, is taken to be Markovian using a generalization of the Langevin equation. This enables information about the structure of the turbulence to be incorporated into the model through the Lagrangian integral time scale, which characterizes the memory of the Lagrangian velocity. At this level of modeling, the particle position is not Markovian (because of the velocity correlation) and the acceleration has a white noise component. This is a reasonable representation of the Lagrangian structure of turbulence at large Reynolds number.[1]

One of the main applications of models of this sort is the prediction of scalar statistics in turbulent flows. Lagrangian theory provides a connection between the displacement statistics of fluid elements (which we refer to as particles) and moments of the scalar field $c(\boldsymbol{x}, t)$ through the relation

$$\langle c\left(\boldsymbol{x}_1, t_1\right) .. c\left(\boldsymbol{x}_n, t_n\right)\rangle = \int_{-\infty}^{t_1} .. \int_{-\infty}^{t_n} \int_V .. \int_V P\left(\boldsymbol{x}_1, t_1, .., \boldsymbol{x}_n, t_n | \boldsymbol{x}'_1, t'_1, .., \boldsymbol{x}'_n, t'_n\right) S\left(\boldsymbol{x}'_1, t'_1\right) .. S\left(\boldsymbol{x}'_n, t'_n\right) d\boldsymbol{x}'_1 .. d\boldsymbol{x}'_n dt'_1 .. dt'_n, \quad (1)$$

where $P\left(\boldsymbol{x}_1, t_1, .., \boldsymbol{x}_n, t_n | \boldsymbol{x}'_1, t'_1, .., \boldsymbol{x}'_n, t'_n\right)$ is the n-particle displacement probability density function (PDF), which is the probability density that a particle is at the position $\boldsymbol{x}_1$ at time t_1, given that it was at the position $\boldsymbol{x}'_1$ at time t'_1, a second particle is at the position $\boldsymbol{x}_2$ at time t_2, given that it was at the position $\boldsymbol{x}'_2$ at time t'_2 etc., and $S\left(\boldsymbol{x}, t\right)$ is the scalar source function.

a)Electronic mail: brian.sawford@monash.edu.

Thus, the mean scalar concentration $\langle c(\boldsymbol{x}, t)\rangle$ is determined by the displacement statistics of a single fluid particle, the mean-square concentration is determined by the joint displacement statistics of two particles and the higher moments of the concentration field are determined by three-particle, four-particle, etc., displacement statistics.

These models are generally presented as a stochastic differential equation (SDE) describing the evolution of the velocity $\boldsymbol{u}(t)$ along a trajectory

$$du_i = a_i(\boldsymbol{u}, \boldsymbol{x}, t)\,dt + b_{ij}(\boldsymbol{u}, \boldsymbol{x}, t)\,dW_j \quad (i, j = 1, 3), \tag{2}$$

where $\boldsymbol{x}(t)$ is the particle position, $\boldsymbol{a}$ is known as the drift term, $\boldsymbol{b}$ is the diffusion coefficient, and $d\boldsymbol{W}$ is the vector incremental Wiener process.[2] The general approach to building these Lagrangian stochastic models (that is, to specifying the drift and diffusion coefficients) is to ensure consistency with as much of the known physics as is possible. Thus, for example, the diffusion coefficient is constrained by requiring that the velocity structure function, $\langle(du_i)^2\rangle$ matches the prediction of Kolmogorov similarity theory[3] for $dt \ll T_L$, where T_L is the Lagrangian integral time scale. This requires the diffusion coefficient to take the form[4,5]

$$b_{ij} = C_0\langle\epsilon\rangle\delta_{ij}, \tag{3}$$

where $\langle\epsilon\rangle$ is the mean rate of dissipation of turbulence kinetic energy, C_0 is the Lagrangian velocity structure function inertial sub-range constant,[3] and $\boldsymbol{\delta}$ is the Kronecker delta.

On the other hand, different approaches have been used to specify the drift term. In the engineering context,[6] plausible assumptions are made about the functional form of the drift coefficient which is then constrained by considering special limiting cases and other physical principles. In addition to predicting Lagrangian and scalar statistics, this approach also predicts the Eulerian statistics of the flow, which provides a demanding test of the efficacy of the modeling.[7] In models developed for environmental applications, the Eulerian statistics of the flow (for example the velocity PDF and $\langle\epsilon\rangle$) are assumed known and are used to constrain the form of the drift term. The culmination of this approach is Thomson's[5] "well-mixed" constraint which ensures that an initially well-mixed scalar field remains so, and preserves the prescribed Eulerian statistics. This is a fundamental and powerful constraint, and is the basis for the models developed in this paper.

Lagrangian stochastic modeling of single particle statistics and the mean scalar field is well advanced and has been applied to a wide range of environmental[8] and engineering flows[6,7,9] including complex flows such as jets, boundary layers, canopy layers, and even strongly non-Gaussian turbulence in convective boundary layers.

Two-particle dispersion, and its modeling, was reviewed by Sawford[10] and more recently by Salazar and Collins.[11] The well-mixed approach has been extended to two-particle models[12,13] in isotropic turbulence, requiring some knowledge of the spatial structure of the flow, which is usually represented by Gaussian velocity statistics and the Eulerian structure function. Non-Gaussian features of the flow have been included,[14,15] but only at the expense of projecting the fully three-dimensional (3D) physics of two-particle dispersion onto a lower-dimensional space using so-called quasi-one-dimensional (Q1D) models. An attempt has also been made to include the effects of intermittency in the Eulerian statistics used to constrain the model.[16] Lüthi *et al.*[17] constructed a stochastic model of relative dispersion by assuming that material line stretching in a modified form can be extended into the inertial sub-range. This approach avoids explicit assumptions about the Eulerian velocity statistics, but requires empirical inputs to fix the "free" parameters. One of the problems with these well-mixed two-particle models is that they are not consistent with the underlying one-particle model; that is, one particle statistics calculated from the two-particle model are not the same as those calculated from the one-particle model.[12,13,18] Kaplan and Dinar[24,25] avoided this problem using an approach in which the Eulerian structure is incorporated through the diffusion term, but Thomson[18] showed that their model does not satisfy the well-mixed constraint.

One of the most fundamental aspects of two-particle dispersion is the rate of separation of the particle pair, which can be characterized most simply by the evolution of the mean-square separation as a function of time. This process, known as relative dispersion, is very important for several reasons. It is fundamentally important because on certain scales, scales much smaller than the scale of the energetic eddies, but much larger than the viscous scales and the scales imposed by the initial

conditions (e.g., the initial separation of the pair of particles), relative dispersion is universal and satisfies Richardson's[19] famous t^3-law

$$\left\langle r^2(t)\right\rangle = g\langle\epsilon\rangle t^3, \tag{4}$$

where r is the separation of the pair of particles and g is a universal constant known as Richardson's constant. At a practical level, relative dispersion controls the dissipation of scalar variance and is thus fundamentally connected with turbulent mixing and concentration fluctuations. It also directly describes the dispersion of puffs and clouds of contaminants. Richardson's constant itself is related to the scalar mixing time scale and controls the transition in relative dispersion from small scales to the independent motion which exists for separations much larger than the large eddies.

Despite its importance, Richardson's law has been very difficult to observe. However, recent analyses of laboratory[20] and direct numerical simulation (DNS)[21,22] data have demonstrated Richardson scaling, with the best estimate being $g \approx 0.5$, only weakly dependent on Reynolds number, for Richardson's constant. All of the well-mixed models we have discussed reproduce Richardson's t^3-law by construction, since the appropriate Kolmogorov scaling is introduced through the specified Eulerian statistics. A definitive test of the models thus reduces to their prediction of Richardson's constant. Fully three-dimensional Gaussian models give values for g close to that observed (see for example, Fig. 3 below), but the non-Gaussian Q1D models give much higher values and are very sensitive to the higher order moments of the prescribed Eulerian velocity statistics. In general the predictions depend greatly on the modeling assumptions. In an attempt to minimize these assumptions, Sawford and Yeung[16] used tabulations of DNS data to define the velocity PDF and the drift term, but were still unable to reproduce the weak Reynolds number dependence of the observed Richardson's constant.[22]

Although two-particle stochastic modeling of relative dispersion remains in an unsatisfactory state, n-particle modeling is still of interest, partly at least because DNS results[23] suggest that the shape statistics of multi-particle clusters more readily show inertial sub-range scaling behavior than does relative dispersion, and that these scaling statistics differ from those generated by particles following independent Gaussian motions. We would like to see for example, how much of this difference is explained by the Gaussian spatial structure of the turbulence, and how much is due to non-Gaussian and n-point aspects of the spatial structure.

The model of Kaplan and Dinar[24,25] is readily extended to n-particles, but fails to give proper Richardson scaling,[18] and as we have noted, is not well-mixed. Here, we focus on the well-mixed approach and extend it to n-particles for Gaussian Eulerian statistics in three-dimensional isotropic turbulence. During the preparation of this article we have become aware of work also extending the well-mixed approach to four particles.[26,27]

The rest of the paper is structured as follows. In Sec. II we present in some detail the theoretical background to the modeling, inertial sub-range scaling, and multi-particle shape statistics. We describe the results of our modeling in Sec. III and our findings are summarized in Sec. IV.

II. THEORY

The models can be formulated in "primitive" coordinates $(\boldsymbol{x}^{(1)}, ..., \boldsymbol{x}^{(n)}, \boldsymbol{u}^{(1)}, ..., \boldsymbol{u}^{(n)})$, where the superscript is a particle label, or in the "reduced" coordinates of Shraiman and Siggia[28] $(\boldsymbol{\rho}^{(0)}, \boldsymbol{\rho}^{(1)}, ..., \boldsymbol{\rho}^{(n-1)}, \boldsymbol{v}^{(0)}, \boldsymbol{v}^{(1)}, ..., \boldsymbol{v}^{(n-1)})$, where the superscript labels the center-of-mass (label 0) and $n-1$ separation variables. Positions in the two coordinate systems are related by the orthogonal transformation

$$\begin{aligned}\boldsymbol{\rho}^{(0)} &= \frac{1}{\sqrt{n}}\sum_{i=1}^{n}\boldsymbol{x}^{(i)},\\ \boldsymbol{\rho}^{(m)} &= \frac{1}{\sqrt{m(m+1)}}\sum_{i=1}^{m}\left(\boldsymbol{x}^{(m+1)} - \boldsymbol{x}^{(i)}\right),\end{aligned} \tag{5}$$

and the $\boldsymbol{v}^{(i)}$ are defined as analogous linear combinations of the $\boldsymbol{u}^{(i)}$,

$$\boldsymbol{v}^{(0)} = \frac{1}{\sqrt{n}} \sum_{i=1}^{n} \boldsymbol{u}^{(i)},$$
$$\boldsymbol{v}^{(m)} = \frac{1}{\sqrt{m(m+1)}} \sum_{i=1}^{m} \left(\boldsymbol{u}^{(m+1)} - \boldsymbol{u}^{(i)} \right), \tag{6}$$

where $m = 1, n-1$. These reduced coordinates have some nice normalization properties and by using them we can formulate the spatial structure in terms of the structure functions rather than the correlation functions, which may have some numerical advantages at small separations. They also are used in defining shape factors for the n-particle cluster.

A. "Well-mixed" models in primitive coordinates

We formulate the models by taking the n-point Eulerian velocity PDF to be joint-Gaussian. In primitive coordinates, we have

$$P_E\left(\boldsymbol{u}^{(1)}, \boldsymbol{u}^{(2)}, \ldots, \boldsymbol{u}^{(n)}\right) = \frac{\lambda^{1/2}}{(2\pi)^{(3n/2)}} \exp\left(-\frac{1}{2} u_i \lambda_{ij} u_j\right) \quad (i, j = 1, 3n), \tag{7}$$

where $\boldsymbol{u} = (u_1^{(1)}, u_2^{(1)}, u_3^{(1)}, \ldots, u_1^{(n)}, u_2^{(n)}, u_3^{(n)})$ is the velocity in $3n$-dimensional velocity phase space. The position coordinates of the n particles are assigned similarly to a $3n$-dimensional phase space. Here our notation neglects the distinction between phase space variables and Lagrangian physical variables, thus avoiding a proliferation of symbols, because in our models quantities such as P_E and its derivatives are evaluated ultimately at the positions and velocities of the particles. Furthermore, our notation is such that vectors and tensors span $3n$-dimensional phase space unless the particle labeling appears explicitly as a superscript, in which case vectors and tensors span 3D space. The turbulence structure is embodied in the pair covariance tensor $\sigma_{ij} = \langle u_i u_j \rangle = \lambda_{ij}^{-1}$ in $3n$-dimensional velocity phase space, where

$$\boldsymbol{\sigma} = \begin{bmatrix} \sigma_u^2 \boldsymbol{\delta} & \boldsymbol{R}^{(12)} & \boldsymbol{R}^{(13)} & \cdots & \boldsymbol{R}^{(1n)} \\ \boldsymbol{R}^{(21)} & \sigma_u^2 \boldsymbol{\delta} & \boldsymbol{R}^{(23)} & \cdots & \boldsymbol{R}^{(2n)} \\ \vdots & \vdots & \vdots & \ddots & \vdots \\ \boldsymbol{R}^{(n1)} & \boldsymbol{R}^{(n2)} & \boldsymbol{R}^{(n3)} & \cdots & \sigma_u^2 \boldsymbol{\delta} \end{bmatrix}, \tag{8}$$

and $R_{ij}^{(mn)}$ is the usual velocity covariance tensor in 3D space evaluated at the positions of the mth and nth particles and is a function of their separation $r^{(mn)} = |\boldsymbol{x}^{(n)} - \boldsymbol{x}^{(m)}|$. The determinant of the inverse covariance tensor in $3n$-dimensional phase space is denoted by λ and the variance of a velocity component is denoted by σ_u^2.

In isotropic turbulence, the 3D covariance tensor is of the form

$$R_{ij}^{(mn)} = \sigma_u^2 \left[(f - g) r_i^{(mn)} r_j^{(mn)} / r^{(mn)^2} + g \delta_{ij} \right], \tag{9}$$

where $f(r^{(mn)})$ and $g(r^{(mn)})$ are the longitudinal and transverse correlation functions, respectively. For incompressible flow $\partial R_{ij}^{(mn)} / \partial r_j^{(mn)} = 0$ so that[29] $g(r) = f(r) + \frac{1}{2} r df/dr$. We approximate $f(r)$ by the interpolation formula[13,30]

$$1 - f(r) = \left(\frac{r^2}{r^2 + L^2} \right)^{1/3}, \tag{10}$$

where $L = \sigma_u^3 / \langle \epsilon \rangle$ is the length scale of the large eddies. Equation (10) satisfies the desired limits

$$f(r) \approx \begin{cases} 1 - C \langle \epsilon \rangle r^{2/3} / 2\sigma_u^2 & (\eta \ll r \ll L) \\ 0 & (r \gg L) \end{cases} \tag{11}$$

with $C = 2$ for the Eulerian velocity structure function constant, which is close to the value 2.13 determined from DNS results.[31]

Stochastic models for the velocities and positions in $3n$-dimensional phase space follow directly from a generalization of the well-mixed results of Thomson[12] in the form given by Borgas and Sawford.[13] They satisfy the SDE

$$\begin{aligned} du_i &= a_i(\boldsymbol{u}, \boldsymbol{x}, t)\, dt + (C_0\langle\epsilon\rangle)^{1/2}\, dW_i, \\ dx_i &= u_i dt \end{aligned} \tag{12}$$

for $i = 1, 3n$.

There is no unique specification for the well-mixed drift term, and a family of quadratic form models, in which the drift is a quadratic function of velocity, was identified by Borgas and Sawford.[13] According to these models, the velocity increments are given by

$$\begin{aligned} du_i &= \frac{1}{2} C_0\langle\epsilon\rangle \frac{\partial \ln P_E}{\partial u_i} dt + \phi_i dt + (C_0\langle\epsilon\rangle)^{1/2}\, dW_i, \\ \phi_i &= \Gamma_i + \gamma_{ijk} u_j u_k. \end{aligned} \tag{13}$$

It can be shown that Γ_i and γ_{ijk} satisfy the equations

$$\Gamma_i \lambda_{ij} u_j - \gamma_{ijk}\left(\delta_{ij} u_k + \delta_{ik} u_j\right) = \frac{1}{2} \lambda^{-1}_{km} \frac{\partial \lambda_{km}}{\partial x_j} u_j \tag{14}$$

and

$$\lambda_{ij}\gamma_{ikl} u_j u_k u_l = -\frac{1}{2} \frac{\partial \lambda_{kl}}{\partial x_j} u_j u_k u_l \tag{15}$$

(see, e.g., Borgas and Sawford[13] Eqs. (4.1a) and (4.1b), but note the sign is wrong on the LHS of (4.1b)). A simple solution for γ_{ijk} follows immediately from Eq. (15) and then substituting into Eq. (14) gives the corresponding solution for Γ_i

$$\begin{aligned} \gamma_{ijk} &= -\frac{1}{2} \lambda^{-1}_{il} \frac{\partial \lambda_{jk}}{\partial x_l}, \\ \Gamma_i &= \frac{1}{2} \lambda^{-1}_{ij} \lambda^{-1}_{km} \frac{\partial \lambda_{km}}{\partial x_j}. \end{aligned} \tag{16}$$

We refer to this model as Borgas's model.

Now, because each of the indices j, k, and l is contracted over the product of velocity components in Eq. (15), we can cyclically permute these indices on the RHS without changing the equation. That is we change $j \to k \to l \to j$ and then obtain the solution

$$\gamma_{ijk} = -\frac{1}{2} \lambda^{-1}_{il} \frac{\partial \lambda_{lk}}{\partial x_j}. \tag{17}$$

Permuting the indices a second time gives the solution

$$\gamma_{ijk} = -\frac{1}{2} \lambda^{-1}_{il} \frac{\partial \lambda_{lj}}{\partial x_k}. \tag{18}$$

This last solution was given by Thomson,[12] and we refer to it by that name. For both Eqs. (17) and (18), $\Gamma_i = 0$. In fact these last two solutions are equivalent since each of the indices j and k is contracted over velocity components in Eq. (13).

In the limit $C_0 \to \infty$, both models reduce to a diffusion process for the positions,[5] which for two particles is essentially equivalent to Richardson's[19] model. In the general case for n particles, this diffusion model is of the form[13]

$$dx_i = \frac{2}{C_0\langle\epsilon\rangle} \frac{\partial \sigma_{ik}\sigma_{kj}}{\partial x_j} dt + \left(\frac{4}{C_0\langle\epsilon\rangle}\right)^{1/2} \sigma_{ij} dW_j \quad (i, j, k = 1, 3n) \tag{19}$$

corresponding to an n-particle diffusivity given by $\kappa_{ij} = 2\sigma_{ik}\sigma_{kj}/C_0\langle\epsilon\rangle$.

B. "Well-mixed" models in reduced coordinates

In reduced coordinates, corresponding to Eq. (7) we have

$$P_E\left(\boldsymbol{v}^{(0)}, \boldsymbol{v}^{(1)}, \ldots, \boldsymbol{v}^{(n-1)}\right) = \frac{\tilde{\lambda}^{1/2}}{(2\pi)^{(3n/2)}} \exp\left(-\frac{1}{2}\upsilon_i \tilde{\lambda}_{ij} \upsilon_j\right) \quad (i, j = 1, 3n), \tag{20}$$

where $\boldsymbol{v} = \left(\upsilon_1^{(0)}, \upsilon_2^{(0)}, \upsilon_3^{(0)}, \upsilon_1^{(1)}, \upsilon_2^{(1)}, \upsilon_3^{(1)}, \ldots \upsilon_1^{(n-1)}, \upsilon_2^{(n-1)}, \upsilon_3^{(n-1)}\right)$ etc. Now the velocity covariance tensor is $\tilde{\sigma}_{ij} = \langle \upsilon_i \upsilon_j \rangle = \tilde{\lambda}_{ij}^{-1}$ and the two models corresponding to Eqs. (13), (16), and (18) are

$$\begin{aligned} d\upsilon_i &= \frac{1}{2} C_0 \langle \epsilon \rangle \frac{\partial \ln P_E}{\partial \upsilon_i} dt + \tilde{\phi}_i dt + (C_0 \langle \epsilon \rangle)^{1/2} dW_i, \\ \tilde{\phi}_i &= \tilde{\Gamma}_i + \tilde{\gamma}_{ijk} \upsilon_j \upsilon_k, \end{aligned} \tag{21}$$

with

$$\begin{aligned} \tilde{\Gamma}_i &= \frac{1}{2} \tilde{\lambda}_{ij}^{-1} \tilde{\lambda}_{km}^{-1} \frac{\partial \tilde{\lambda}_{km}}{\partial \rho_j}, \\ \tilde{\gamma}_{ijk} &= -\frac{1}{2} \tilde{\lambda}_{il}^{-1} \frac{\partial \tilde{\lambda}_{jk}}{\partial \rho_l} \end{aligned} \tag{22}$$

for Borgas' model, and

$$\begin{aligned} \tilde{\Gamma}_i &= 0, \\ \tilde{\gamma}_{ijk} &= -\frac{1}{2} \tilde{\lambda}_{il}^{-1} \frac{\partial \tilde{\lambda}_{lj}}{\partial \rho_k} \end{aligned} \tag{23}$$

for Thomson's model.

The diffusion limit corresponding to Eq. (21) is simply

$$d\rho_i = \frac{2}{C_0 \langle \epsilon \rangle} \frac{\partial \tilde{\sigma}_{ik} \tilde{\sigma}_{kj}}{\partial \rho_j} dt + \left(\frac{4}{C_0 \langle \epsilon \rangle}\right)^{1/2} \tilde{\sigma}_{ij} dW_j \qquad (i, j, k = 1, 3n). \tag{24}$$

In order to complete the specification of the models in reduced coordinates, we need to write the covariance tensor $\tilde{\sigma}_{ij}$ in terms of the usual covariance tensors in 3D space R_{ij}^{mn}. Partitioning $\tilde{\sigma}_{ij}$ in terms of the 3D tensors $\tilde{R}_{ij}^{(mn)} = \left\langle \upsilon_i^{(m)} \upsilon_j^{(n)} \right\rangle$, corresponding to Eq. (8) we have

$$\tilde{\boldsymbol{\sigma}} = \begin{bmatrix} \tilde{\boldsymbol{R}}^{(00)} & \tilde{\boldsymbol{R}}^{(01)} & \tilde{\boldsymbol{R}}^{(02)} & \cdots & \tilde{\boldsymbol{R}}^{(0(n-1))} \\ \tilde{\boldsymbol{R}}^{(10)} & \tilde{\boldsymbol{R}}^{(11)} & \tilde{\boldsymbol{R}}^{(12)} & \cdots & \tilde{\boldsymbol{R}}^{(1(n-1))} \\ \vdots & \vdots & \vdots & \ddots & \vdots \\ \tilde{\boldsymbol{R}}^{((n-1)0)} & \tilde{\boldsymbol{R}}^{((n-1)1)} & \tilde{\boldsymbol{R}}^{((n-1)2)} & \cdots & \tilde{\boldsymbol{R}}^{((n-1)(n-1))} \end{bmatrix}. \tag{25}$$

The component covariances are, from Eq. (6),

$$\tilde{R}_{ij}^{(00)} = \frac{1}{n} \sum_{l=1}^{n} \sum_{m=1}^{n} \left\langle u_i^{(l)} u_j^{(m)} \right\rangle = \sigma_u^2 \delta_{ij} + \frac{2}{n} \sum_{l=1}^{n} \sum_{m=l+1}^{n} R_{ij}^{(lm)}, \tag{26}$$

$$\begin{aligned} \tilde{R}_{ij}^{(0m)} &= \frac{1}{\sqrt{nm(m+1)}} \sum_{k=1}^{n} \sum_{l=1}^{m} \left(\left\langle u_i^{(k)} u_j^{(m+1)} \right\rangle - \left\langle u_i^{(k)} u_j^{(l)} \right\rangle \right) \\ &= \frac{1}{\sqrt{nm(m+1)}} \sum_{k=1}^{n} \sum_{l=1}^{m} \left(R_{ij}^{(k(m+1))} - R_{ij}^{kl} \right) \\ &= \frac{-1}{2\sqrt{nm(m+1)}} \sum_{k=1}^{n} \sum_{l=1}^{m} \left(D_{ij}^{(k(m+1))} - D_{ij}^{kl} \right), \end{aligned} \tag{27}$$

$$\widetilde{R}_{ij}^{(lm)} = \frac{1}{\sqrt{l(l+1)m(m+1)}} \sum_{k=1}^{l}\sum_{p=1}^{m} \left\langle \left(u_i^{(l+1)} - u_i^{(k)}\right)\left(u_j^{(m+1)} - u_j^{(p)}\right)\right\rangle$$
$$= \frac{1}{\sqrt{l(l+1)m(m+1)}} \sum_{k=1}^{l}\sum_{p=1}^{m} \left(R_{ij}^{((l+1)(m+1))} - R_{ij}^{(k(m+1))} - R_{ij}^{((l+1)p)} + R_{ij}^{(kp)}\right)$$
$$= \frac{-1}{2\sqrt{l(l+1)m(m+1)}} \sum_{k=1}^{l}\sum_{p=1}^{m} \left(D_{ij}^{((l+1)(m+1))} - D_{ij}^{(k(m+1))} - D_{ij}^{((l+1)p)} + D_{ij}^{(kp)}\right), \quad (28)$$

where $D_{ij}^{(pq)} = 2\left(\sigma_u^2\delta_{ij} - R_{ij}^{(pq)}\right)$ is the 3D structure function and l, $m > 0$. Note that we can write Eqs. (27) and (28) in terms of the structure functions because there are equal numbers of covariance terms with positive and negative signs, so we can subtract a delta function term from each covariance term without changing the result. In principle, for small separations it is better to use reduced coordinates because then the separation velocity increment is calculated directly, rather than as the difference of two nearly equal increments for the two particles. In practice, there seems to be no significant difference between separation statistics calculated in primitive coordinates and those calculated in reduced coordinates. Since the primitive equations are simpler, we have used those.

C. Inertial sub-range scaling

Following Thomson,[12] and Borgas and Sawford,[32] we focus on the single particle difference variables $\delta\boldsymbol{u}^{(m)} = \boldsymbol{u}^{(m)}(t) - \boldsymbol{u}^{(m)}(0)$ and $\delta\boldsymbol{x}^{(m)} = \boldsymbol{x}^{(m)}(t) - \boldsymbol{u}^{(m)}(0)t - \boldsymbol{x}^{(m)}(0)$, two-particle difference variables, $\delta\boldsymbol{u}^{(mn)} = \delta\boldsymbol{u}^{(n)} - \delta\boldsymbol{u}^{(m)}$ and $\delta\boldsymbol{r}^{(mn)} = \delta\boldsymbol{x}^{(n)} - \delta\boldsymbol{x}^{(m)}$ and corresponding reduced quantities, $\delta\boldsymbol{v}^{(m)} = \boldsymbol{v}^{(m)}(t) - \boldsymbol{v}^{(m)}(0)$ and $\delta\boldsymbol{\rho}^{(m)} = \boldsymbol{\rho}^{(m)}(t) - \boldsymbol{v}^{(m)}(0)t - \boldsymbol{\rho}^{(m)}(0)$, which have the scaling behaviour

$$\left\langle \left(\delta u_i^{(m)}\right)^2\right\rangle = 3C_0\langle\epsilon\rangle t \qquad \left(t_\eta \ll t \ll T_L\right),$$
$$\left\langle \left(\delta x_i^{(m)}\right)^2\right\rangle = C_0\langle\epsilon\rangle t^3 \qquad \left(t_\eta \ll t \ll T_L\right) \quad (29)$$

for single particle differences,

$$\left\langle \left(\delta u_i^{(mn)}\right)^2\right\rangle = \begin{cases} 6C_0\langle\epsilon\rangle t & (t \ll t_0 \ll T_L) \\ g_u\langle\epsilon\rangle t & (t_0 \ll t \ll T_L) \end{cases} \quad (30)$$

for relative velocity differences, where $g_u = 6C_0 - 4C_1$,

$$\left\langle \left(\delta r_i^{(mn)}\right)^2\right\rangle = \begin{cases} 2C_0\langle\epsilon\rangle t^3 & (t \ll t_0 \ll T_L) \\ g\langle\epsilon\rangle t^3 & (t_0 \ll t \ll T_L) \end{cases} \quad (31)$$

for separation differences, where $g = 2C_0 - 2C_1 + \frac{2}{3}C_2$,

$$\left\langle \left(\delta v_i^{(m)}\right)^2\right\rangle = \begin{cases} 3C_0\langle\epsilon\rangle t & (t \ll t_0 \ll T_L) \\ \frac{1}{2}g_u\langle\epsilon\rangle t & (t_0 \ll t \ll T_L) \end{cases} \quad (32)$$

for reduced separation velocity differences ($m \geq 1$), and

$$\left\langle \left(\delta \rho_i^{(m)}\right)^2\right\rangle = \begin{cases} C_0\langle\epsilon\rangle t^3 & (t \ll t_0 \ll T_L) \\ \frac{1}{2}g\langle\epsilon\rangle t^3 & (t_0 \ll t \ll T_L) \end{cases} \quad (33)$$

for reduced separations with $m \geq 1$. In these scaling relations $t_0 = r_0^{2/3}\langle\epsilon\rangle^{-1/3}$, where r_0 is the initial separation, is the Batchelor time scale[33] which represents the time for which the memory of the initial conditions persists, and T_L is the Lagrangian integral time scale. The two-particle scaling relations in Eqs. (30)–(33) also require $\eta \ll r_0$.

The constant g is Richardson's constant and g_u is the corresponding constant for the relative velocity in the Richardson scaling range $t_0 \ll t \ll T_L$. In the Batchelor range $t \ll t_0$, the covariance between the accelerations of particle pairs is negligible[3,12,32] so they move independently and the corresponding scaling constants in Eqs. (30)–(33) are simply related to the single particle results in Eq. (29). The constants C_1 and C_2 are defined in terms of the inertial sub-range properties of the two-particle acceleration covariance[32]

$$C_1 = \int_0^1 \chi^{-1} R_2^{(A)}(\chi)\, d\chi,$$
$$C_2 = \int_0^1 R_2^{(A)}(\chi)\, d\chi, \tag{34}$$

where, for times ($t_0 \ll t_1, t_2 \ll T_L$),

$$R_2^{(A)}(t_1/t_2) = \left\langle A_i^{(1)}(t_1)\, A_i^{(2)}(t_2) \right\rangle / \left(\langle \epsilon \rangle t_1^{-1} \right), \tag{35}$$

$\boldsymbol{A}^{(m)}$ is the acceleration of the mth particle and $R_2^{(A)}$ is the inertial sub-range compensated two-particle acceleration correlation.

Now it can be shown simply by expanding the summations in the definitions of the reduced variables that

$$\sum_{m=1}^{n} \left\langle \left(\delta x_i^{(m)} \right)^2 \right\rangle = \sum_{m=0}^{n-1} \left\langle \left(\delta \rho_i^{(m)} \right)^2 \right\rangle = \left\langle \left(\delta \rho_i^{(0)} \right)^2 \right\rangle + \sum_{m=1}^{n-1} \left\langle \left(\delta \rho_i^{(m)} \right)^2 \right\rangle \tag{36}$$

and substituting the scaling results from Eqs. (29)–(33) we find that the center-of-mass scales like

$$\left\langle \left(\delta \rho_i^{(0)} \right)^2 \right\rangle = \begin{cases} C_0 \langle \epsilon \rangle t^3 & (t \ll t_0 \ll T_L) \\ \left(nC_0 - \frac{1}{2}(n-1)\, g \right) \langle \epsilon \rangle t^3 & (t_0 \ll t \ll T_L) \end{cases}. \tag{37}$$

Similarly, the center-of-mass velocity difference scales like

$$\left\langle \left(\delta v_i^{(0)} \right)^2 \right\rangle = \begin{cases} 3C_0 \langle \epsilon \rangle t & (t \ll t_0 \ll T_L) \\ \left(3nC_0 - \frac{1}{2}(n-1)\, g_u \right) \langle \epsilon \rangle t & (t_0 \ll t \ll T_L) \end{cases}. \tag{38}$$

Richardson scaling for the relative dispersion, is identified and quantified by plotting the so-called cubed local slope (CLS) $(d\langle(\delta y_i)^2\rangle^{1/3}/dt)^3$, where $\boldsymbol{y}$ can be any of $\boldsymbol{x}^{(m)}$, $\boldsymbol{\rho}^{(m)}$, or $\boldsymbol{r}^{(lm)}$ or the corresponding difference variables, as a function of $\log(t)$ as illustrated in Fig. 1 which shows the CLS of the mean-square separation difference of a pair of particles. There we see two regions growing like t^3 (corresponding to those in Eq. (31)) which appear as plateaus. For $t \ll t_0$ the CLS approaches the Batchelor-range independent motion limit $2C_0 = 14$, while in the Richardson scaling range $t_0 \ll t \ll T_L$ there is a clear plateau at the value $g = 1.08$ for the Richardson constant.

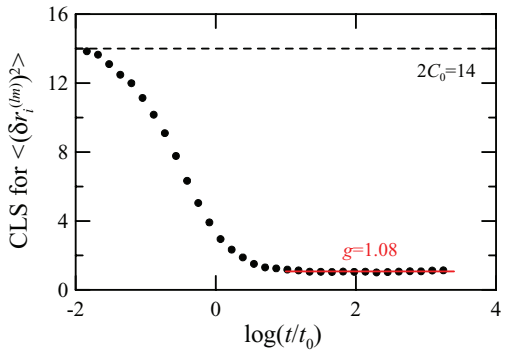

FIG. 1. Cubed local slope plot of difference relative dispersion. Dashed line is Batchelor range independent motion limit $2C_0 = 14$ and solid red line is a fit to the Richardson range (here with $g = 1.08$).

1. Diffusion limit

Analytical solutions are possible for Richardson's diffusion model in the inertial sub-range; i.e., for Eq. (19) with $n = 2$. The relative dispersion is given by $\langle r^2 \rangle = \sigma_r^2 = g\langle\epsilon\rangle t^3$ with

$$g = \frac{1144C^6}{81C_0^3}. \tag{39}$$

The separation PDF is given by

$$P(r/\sigma_r) = \left(\frac{1144}{81}\right)^{3/2} \left(\frac{2187}{560}\right) \pi^{-1/2} \left(\frac{r}{\sigma_r}\right)^2 \exp\left[-\frac{9}{4}\left(\frac{1144}{81}\right)^{1/3} \left(\frac{r}{\sigma_r}\right)^{2/3}\right], \tag{40}$$

which is normalized so that $\int_0^\infty P(r)\,dr = 1$. This is often presented as the so-called distance-neighbour function, defined here as $q(r/\sigma_r) = P(r/\sigma_r)/(r/\sigma_r)^2$. For convenience here we have dropped the particle labeling superscripts in our notation. Note, that as defined here σ_r^2 is the mean-square separation, not the square of the standard deviation, since the mean magnitude of the separation $\langle r \rangle$ is not zero.

D. Shape statistics

We form the $3 \times (n-1)$ matrix whose columns are the $n-1$ separation vectors $\boldsymbol{\rho}^{(m)}$

$$\boldsymbol{\rho} = \begin{bmatrix} \rho_1^{(1)} & \rho_1^{(2)} & \cdots & \rho_1^{(n-1)} \\ \rho_2^{(1)} & \rho_2^{(2)} & \cdots & \rho_2^{(n-1)} \\ \rho_3^{(1)} & \rho_3^{(2)} & \cdots & \rho_3^{(n-1)} \end{bmatrix} \tag{41}$$

and then take the products $\boldsymbol{\rho}\boldsymbol{\rho}^T$ and $\boldsymbol{\rho}^T\boldsymbol{\rho}$ which are known as the 3×3 moment of inertia and $(n-1) \times (n-1)$ dispersion tensors, respectively. These two tensors can be diagonalized and each has the same $\min(n-1, 3)$ non-zero eigenvalues $g_1, g_2 \ldots$ in order of decreasing magnitude. Thus for three particles forming a triangle there are two non-zero eigenvalues, while for $n \geq 4$ there are three non-zero eigenvalues. The sum of the eigenvalues is the square of the so-called gyration radius $R^2 = g_1 + g_2 + \ldots$, but could also be identified as the squared separation averaged over all possible separations in the n-particle cluster

$$R^2 = \frac{1}{2n} \sum_{l,m=1}^{n} \left(x_i^{(m)} - x_i^{(l)}\right)^2. \tag{42}$$

Thus R is a measure of the size of the n-particle cluster.

The ratios $I_i = g_i/R^2$ are measures of the shape of the cluster and satisfy the constraint $\sum I_i = 1$. For triangles, I_1 and I_2 are related to the aspect ratio, defined as the area A of the triangle to the area of an equilateral triangle of the same scale, $w = 4A/\sqrt{3R^2}$, through the relations $I_2 = \frac{1}{2}\left(1 - \sqrt{1-w^2}\right)$ and $I_1 = 1 - I_2$. Similarly for tetrads and higher order clusters, the shape factors are related to two measures of the aspect ratio based on relations between volume and scale and surface area and scale.[23]

The matrix $\boldsymbol{\rho}$ can also be represented by the singular value decomposition[34]

$$\rho_i^{(m)} = \mathcal{R}_{ik}\mathcal{S}_k^{(l)}\mathcal{R}^{T^{(l)(m)}}, \tag{43}$$

where $\mathcal{R}_{ij}$ represents a rotation in three-dimensional physical space, $\mathcal{R}^{(l)(m)}$ represents a rotation in $(n-1)$-dimensional particle labeling space and $\mathcal{S}_k^{(l)}$ represents a scaling along the rotated axes. $\mathcal{S}_k^{(l)}$ is diagonal and its non-zero elements are just the square roots of the non-zero eigenvalues of $\boldsymbol{\rho}\boldsymbol{\rho}^T$ and $\boldsymbol{\rho}^T\boldsymbol{\rho}$. In other words, the rotations in physical and particle labeling space are orthogonal transformations that diagonalize $\boldsymbol{\rho}$.

Rotations in physical space clearly relate to the orientation, rather than the shape, of the cluster of particles. However, the rotation in labelling space, characterized by $(n-1)(n-2)/2$ Euler angles,

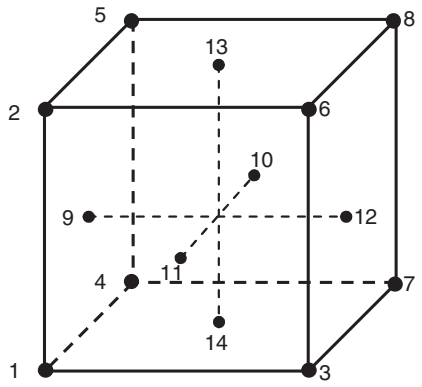

FIG. 2. Schematic of initial positions for $n \leq 14$ particles.

carries information about the symmetry of the cluster. For example, the single Euler angle,[28]

$$\chi = \frac{1}{2}\arctan\left(\frac{2\boldsymbol{\rho}^{(1)}\cdot\boldsymbol{\rho}^{(2)}}{\left|\boldsymbol{\rho}^{(2)}\right|^2-\left|\boldsymbol{\rho}^{(1)}\right|^2}\right) \tag{44}$$

for a triangle in two-dimensional particle labeling space, say, is a measure of the departure from an isosceles shape. It covers the range $0 \leq \chi \leq \pi/6$, with $\chi = 0$ corresponding to isosceles triangles with two sides shorter than the third, and $\chi = \pi/6$ corresponding to isosceles triangles with two sides longer than the third.[23,35,36]

III. NUMERICAL RESULTS

The n-particle code was initialized for up to fourteen particles with each particle at the vertex or the center of a face of a cube with sides of length r_0 as illustrated in Fig. 2, and for $n \leq 14$, the particles are chosen in numerical order of the labeling. Thus, for three particles, the initial configuration is a right isosceles triangle with vertices at $\boldsymbol{x}^{(1)} = (-1, -1, -1)r_0/2$, $\boldsymbol{x}^{(2)} = (-1, -1, 1)r_0/2$ and $\boldsymbol{x}^{(3)} = (1, -1, -1)r_0/2$ and for four particles it is a right tetrahedron as in the DNS results of Hackl *et al.*,[23] with $\boldsymbol{x}^{(4)} = (-1, 1, -1)r_0/2$. In order to generate a suitably long Richardson scaling range, the initial separation scale was chosen for most runs as $r_0 = 10^{-9}L$. The SDEs were integrated using a first order Euler scheme with an adaptive time step $\Delta t/T_E = \Delta t_{con}(r/L)^{2/3}$, where $T_E = L/\sigma_u$ is the Eulerian time scale of the large eddies, that is designed to resolve the inertial sub-range motions. The integration was typically terminated at $t/t_0 \approx 2.5 \times 10^3$ which is equivalent to $t/T_L \approx 8.8 \times 10^{-3}$. This gives a Richardson range extending over two orders of magnitude in time, as illustrated in Fig. 1. Dispersion statistics are written to file at logarithmically spaced time intervals $t/t_0 = 3^{(n_p-1)/3} \times 10^{-2}$ for $n_p = 1, 35$. Some calculations were also performed with a separate three-particle code with the particles initially at the vertices of an equilateral triangle with sides of length r_0.

Statistical sampling uncertainty was estimated from an ensemble of ten runs each of $N = 1000$ realizations for both $n = 2$ and $n = 3$. Tests for two- and three-particle models at $C_0 = 7$ give standard errors for 10^4 samples of 1% on the estimate for g, 0.03% for the shape factor I_1, and 0.3% for the shape factor I_2.

Tests of finite differencing accuracy show that results for g converge to within 1% for a time step with $\Delta t_{con} = 0.005$. Tests also show no significant difference in results calculated in primitive or reduced coordinates.

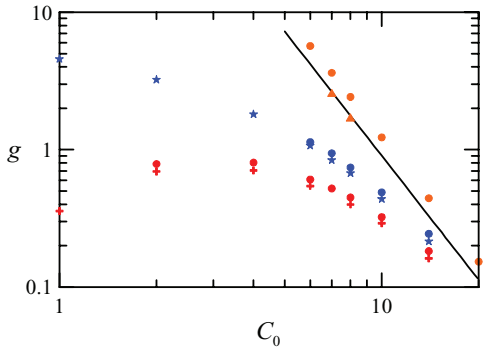

FIG. 3. Model estimates of Richardson's constant as a function of C_0. Symbols are (bottom to top) for Borgas two-particle model (red cross), Borgas three-particle model (red circle), Thomson two-particle model (blue star), Thomson three-particle model (blue circle), diffusion two-particle model (orange triangle), and diffusion three-particle model (orange circle). The solid line is the analytical result (Eq. (39)) for the two-particle diffusion model.

A. Dispersion statistics

1. Mean-square dispersion

First we examine the relative dispersion predictions, i.e., $\langle r^2(t)\rangle$ and in particular Richardson's constant g. Figure 3 shows values of Richardson's constant as a function of the Lagrangian velocity structure function constant C_0 for various models as indicated in the caption. We keep the Eulerian velocity structure function constant fixed at $C = 2$.

The two-particle results for both Borgas' model (Eq. (16)) and Thomson's model (Eq. (18)) are close to those presented in Fig. 9 of Borgas and Sawford.[13] The corresponding three-particle models give values for g about 10% larger than the two-particle models. This is not surprising and is a result of the lack of proper reduction to lower order in these models; i.e., the modelling approach does not guarantee that one- or two-particle statistics calculated from the three-particle model will be the same as those from a one- or two-particle model, a generalisation of the discrepancy noted with regard to two-particle models in Sec. I. Figure 3 also shows results for g for the diffusion equation (19) for both the two-particle case, where there is an analytical result (Eq. (39)), and the three-particle case. The three-particle diffusion result is 35% larger than the two-particle result, much larger than the difference for Thomson's and Borgas' models.

We have estimated g as a function of n for Thomson's model and for the diffusion equation for $C_0 = 7$ and 14. The results are shown in Fig. 4. We see that g increases strongly with n, especially for the diffusion equation. In fact, the increase is exponential $g = g_0 \exp(\alpha n)$ as shown by the lines fitted to the numerical results which are shown by the symbols. The growth rate α for the diffusion

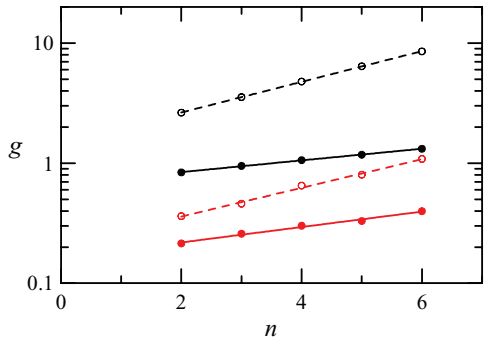

FIG. 4. Richardson's constant g estimated for Thomson's model (filled symbols; solid lines) and the diffusion equation (open symbols; dashed lines) as a function of the number of particles n. Upper two (black) lines are for $C_0 = 7$, and the lower two (red) lines are for $C_0 = 14$.

equation is independent of C_0 (0.276 ± 0.001 for both $C_0 = 7$ and 14), but for Thomson's model increases from 0.112 for $C_0 = 7$ to 0.146 for $C_0 = 14$. This increase in the growth rate with increasing C_0 is a consequence of the fact that Thomson's model approaches the diffusion model in the limit $C_0 \to \infty$. As n increases for finite values of C_0, the gap between g estimated from Thomson's model and the diffusion model increases and increasingly large values of C_0 are needed in order for Thomson's model to approach the diffusion limit.

This strong increase in Richardson's constant with increasing n is an unwanted feature of these models, since it implies, for example, that the scalar dissipation varies strongly with n, and therefore that these models will not give sensible estimates for higher-order concentration moments. While this is clearly unsatisfactory at a fundamental level, it has been suggested[26] that at a practical level C_0 might be treated as an adjustable parameter and tuned to give the correct value of g. Our results show that a suitable value of C_0 would need to be an increasing function of n since g is over-predicted increasingly with increasing n. However, the effective value of C_0 in these models is also constrained by the single particle dispersion in the far field, which generally[37] requires a value $C_0 < 7$. Accommodating these conflicting requirements is difficult.

Some insight into this unsatisfactory behaviour can be inferred from inertial sub-range scaling of the center-of-mass. We have already deduced the correct scaling of the center-of-mass difference statistics in Eqs. (37) and (38). Thomson[12] showed that for his model for the center-of-mass velocity difference, i.e., Eqs. (21) and (23) with $i = 1$, 2, or 3 and $n = 2$, in the inertial sub-range, the leading order term is the diffusion term

$$d\delta v_i^{(0)} \sim \sqrt{C_0\langle\epsilon\rangle}\, dW_i^{(0)} \qquad (t \ll T_L), \tag{45}$$

so that

$$\left.\begin{aligned} \left\langle \left(\delta v_i^{(0)}\right)^2 \right\rangle &\sim 3C_0\langle\epsilon\rangle t \\ \left\langle \left(\delta \rho_i^{(0)}\right)^2 \right\rangle &\sim C_0\langle\epsilon\rangle t^3 \end{aligned}\right\} \qquad (t \ll T_L)\,, \tag{46}$$

which differ significantly from the correct scaling constants in Eqs. (37) and (38) in the Richardson range. That is, there is no impact of the drift term on the center-of-mass statistics in the Richardson range. We have confirmed these results numerically and shown, also numerically, that they can be extended to $n > 2$. As a result of this discrepancy, it follows that the model gives the incorrect scaling coefficients for the one-particle difference statistics in the Richardson range. For example, substituting from Eqs. (33) and (46) into Eq. (36) we get

$$\left\langle \left(\delta x_i^{(m)}\right)^2 \right\rangle = \begin{cases} C_0\langle\epsilon\rangle t^3 & (t \ll t_0 \ll T_L) \\ \left(C_0 + \frac{1}{2}(n-1)\, g\right)\langle\epsilon\rangle t^3 & (t_0 \ll t \ll T_L) \end{cases} \tag{47}$$

compared with Eq. (29).

Thus, it seems that in some sense the models put too much energy into the separation process and not enough into the center-of-mass dispersion, and that this gets worse with increasing n. One might expect though, that this effect would be algebraic in n, whereas we see an exponential increase in g.

2. Relative dispersion PDFs

It is very common to compare experimental or numerical estimates for the pair separation PDF with the predictions of Richardson's diffusion model (Eq. (40)) in order to assess the extent to which relative dispersion is a diffusion process. We find here that the well-mixed class of models is certainly not diffusive for realistic values[38] of $C_0 \sim 7$ since the estimates for g depart significantly from the diffusion equation estimates. Somewhat surprisingly, however, the well-mixed models show a scaling range for $t_0 \ll t \ll T_L$ in which the separation PDF matches Richardson's PDF (Eq. (40)). This applies for both the Thomson and Borgas models and for all values of n. Figure 5 illustrates this result for $n = 4$, a run where we used 10^5 particles in order to improve the sampling.

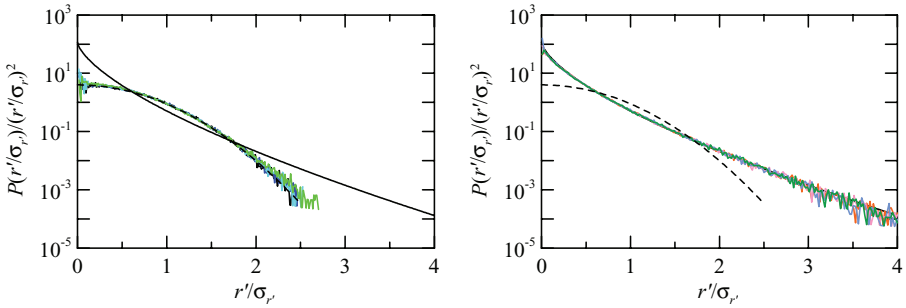

FIG. 5. Richardson's distance-neighbour function estimated for Thomson's model for $n = 4$ for a range of times. Left panel shows times $t \leq 0.27t_0$ and right panel shows times $t \geq 7.29t_0$ (in both cases the precise order is not important). The initial separation has been subtracted, $r' = r_i - r_{i0}$, and the results are averaged over all separations in the cluster. Richardson's result from Eq. (40) is plotted as a solid black line, which is almost completely obscured by the model results in the right panel. The dashed line is a Gaussian function and is almost completely obscured by the model results in the left panel.

At small times, as shown in the left panel, the deviation in the separation from its initial value is close to Gaussian. For times within the Richardson scaling range, $t_0 \ll t \ll T_L$, the numerical results collapse almost exactly onto the Richardson result as shown in the right panel. We conclude that agreement with Eq. (40) is not necessarily an indication that the underlying process is diffusive.

As an aside here, we present some results for a model which has been constructed deliberately to violate the well-mixed constraint, in order to illustrate the importance of that constraint. For this purpose, we take Borgas' model Eq. (16) and set the constant part of the drift term to zero, $\Gamma_i = 0$. We find for $C_0 = 6$ that this "un-mixed" model gives a value $g = 1.11$ for Richardson's constant, twice as large as that for the corresponding well-mixed model. The effects of un-mixing in this model are shown clearly in the distribution of separations. Figure 6 shows both the distance-neighbour function and the separation PDF for times in the Richardson scaling range. The main effect of un-mixing is a deficit of small separations and an increase of separations of order $\sigma_{r'}$. There is also a weak deficit of large separations.

B. Shape statistics

1. Triangles

We commence with results for the shape statistics of the triangles formed by three particles. The left panel in Fig. 7 shows results for mean shape factors $\langle I_1 \rangle$ and $\langle I_2 \rangle$ for both Thomson's model Eq. (18) and Borgas' model Eq. (16) with $C_0 = 7$. The results for the two models are so close that they are virtually indistinguishable. In the Richardson range, $t_0 \ll t \ll T_L$ the model results

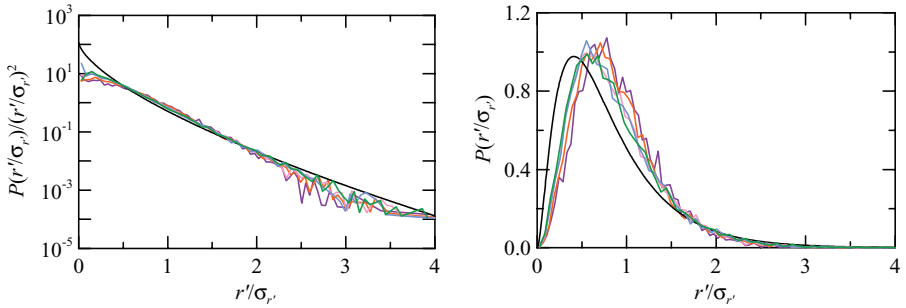

FIG. 6. Richardson's distance-neighbour function (left panel) estimated for "un-mixed" version of Borgas' model for $n = 2$ and a range of times $t \geq 7.29t_0$ (the precise order is not important), representative of the Richardson scaling range. The initial separation has been subtracted, $r' = (r_i - r_{i0})$. Richardson's result from Eq. (40) is plotted as a solid black line. Right panel shows the corresponding PDF in linear coordinates.

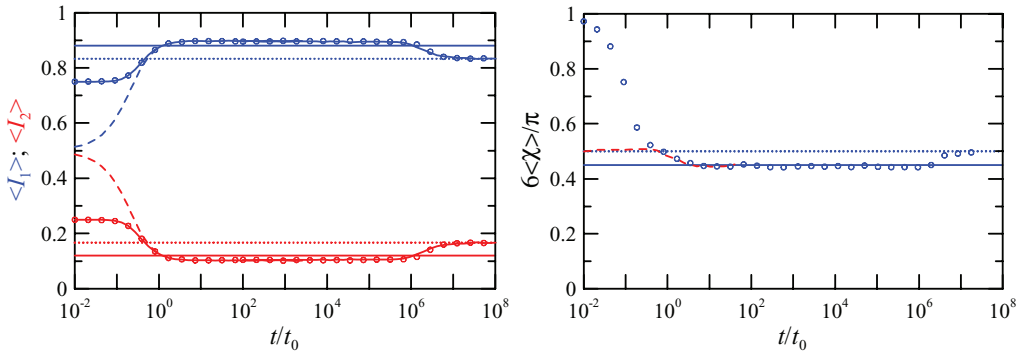

FIG. 7. Model estimates of mean shape statistics for triangles as a function of non-dimensional time for an initial separation $r_0/L = 10^{-9}$ and $C_0 = 7$, corresponding to $t_0/T_L = \frac{1}{2}C_0(r_0/L)^{2/3} = 3.5 \times 10^{-6}$. Left panel: the mean shape factors $\langle I_1\rangle$ and $\langle I_2\rangle$. Open red circles and (overlapping) solid red curve (lower) are $\langle I_2\rangle$ for Borgas and Thomson models, respectively, for initially right isosceles triangles and open blue circles and (overlapping) solid blue line (upper) are corresponding results for $\langle I_1\rangle$. The red and blue dashed curves are for Thomson's model for initially equilateral triangles. The solid horizontal lines are DNS estimates in the inertial sub-range ($\langle I_1\rangle = 0.88$ and $\langle I_2\rangle = 0.12$) and the dotted horizontal lines are the analytical independent motion estimates ($\langle I_1\rangle = 5/6$ and $\langle I_2\rangle = 1/6$). Right panel: the mean symmetry parameter $\langle\chi\rangle$. Blue circles are for Borgas' model for initially right isosceles triangles and the dashed red curve is for Thomson's model for initially equilateral triangles. The solid horizontal line is the DNS estimate in the inertial sub-range ($6\langle\chi\rangle/\pi = 0.45$) and the dotted horizontal line is the Monte Carlo independent motion estimate ($6\langle\chi\rangle/\pi = 1/2$).

($\langle I_1\rangle = 0.90$; $\langle I_2\rangle = 0.1$) deviate only slightly from the DNS results ($\langle I_1\rangle = 0.88$; $\langle I_2\rangle = 0.12$) shown as horizontal solid lines and, as expected, at large times approach the independent motion limit shown as the horizontal dotted lines. By comparing the results for Thomson's model for initially right isosceles triangles (solid curves) and initially equilateral triangles (dashed curves), it can be seen that the effect of the initial conditions persists for a period of order $t \sim t_0$ and for later times, in the Richardson range and beyond, the results are independent of the initial configuration. Figure 7 also shows results for the mean of the symmetry parameter $\langle\chi\rangle$ in the right panel. For clarity we show results for Borgas' model only for initially right isosceles triangles and for Thomson's model for initially equilateral triangles, and we see that the models are in almost perfect agreement with the DNS results in the Richardson range. Results for the initially equilateral triangles approach the limit $6\langle\chi\rangle/\pi$ at both small times (due to the indeterminacy of χ for equilateral triangles) and large times (where the particle motion is independent) as also observed in DNS results.[23] Again, the initial configuration affects the results only for a period of order t_0.

We see that the pair-wise Gaussian physics in these models gives a good representation of the mean inertial sub-range shape dynamics capturing most of the deviation from the independent motion limit. This suggests that non-Gaussian effects and three-point spatial correlations are of relatively minor importance. Clearly this is most encouraging from a practical modeling point of view. It is interesting to see that both models give essentially the same mean shape statistics.

Figure 8 shows PDFs of these shape statistics for Thomson's model for initially right isosceles triangles. For the shape factor I_1 shown in the left panel the initial condition is a delta function at $I_1 = 3/4$. In the early stages of its evolution ($t/t_0 = 0.1$), the PDF spreads roughly symmetrically about the initial delta function, and then at later times ($t/t_0 = 0.3$) the peak value moves towards larger I_1. The effects of the initial condition persist until $t/t_0 \approx 1$ after which, within the Richardson scaling regime, all the curves collapse to a single curve which increases strongly and monotonically over the range $0.5 \le t/t_0 \le 1$. The PDF of the symmetry parameter χ shows a similar rapid evolution from its initial value $\delta(\chi - \pi/6)$ to a scaling form which decreases monotonically over its range. For both I_1 and χ the model PDFs are close to the DNS PDFs shown as the dashed black lines and differ significantly from the independent Gaussian motion limit shown as the blue dotted lines. Thus, even at this detailed level, we see that pair-wise Gaussian physics does a very good job of representing inertial sub-range shape dynamics.

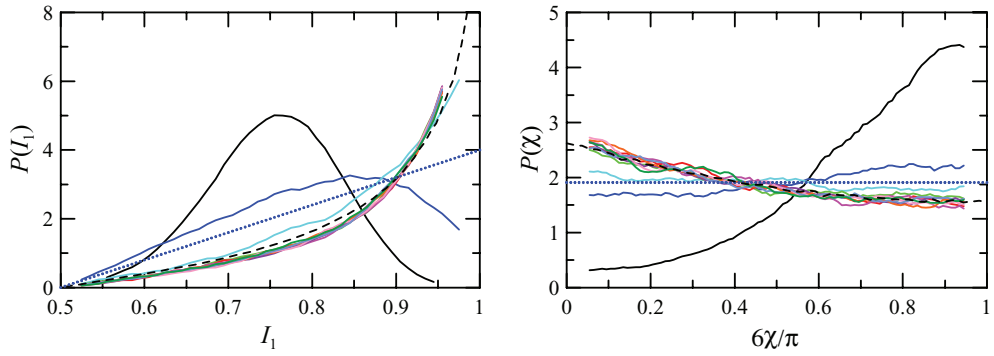

FIG. 8. Model estimates for the PDFs of shape statistics for initially right isosceles triangles for an initial separation $r_0/L = 10^{-9}$ and $C_0 = 7$. Left panel: the shape factor I_1, for which the initial condition is a delta function at $I_1 = 3/4$, for a range of non-dimensional times $t/t_0 = 0.1$ (black curve with peak at $I_1 \approx 0.75$), 0.3 (blue curve with peak at $I_1 \approx 0.85$), 0.9 (cyan curve just above the dashed curve), 2.7, . . . , 5.9×10^3 (remaining curves collapsing to a self-similar form). The black dashed line is the average over Richardson scaling times from DNS and the blue dotted line is the independent motion diffusive limit. Right panel: the triangle symmetry parameter χ for which the initial condition is a delta function at $\chi = \pi/6$, for a range of non-dimensional times $t/t_0 = 0.1$ (black curve with $P(\chi)$ ranging from 0.4 to 4.5), 0.3 (blue curve with $P(\chi)$ ranging from 1.7 to 2.3), 0.9 (cyan curve close to the blue dotted line), 2.7, . . . , 5.9×10^3 (remaining curves collapsing to a self-similar form). The dashed and dotted lines are as in the left panel.

2. Tetrads

Mean shape factors for tetrads are shown in Fig. 9 for both Thomson's model and the diffusion model. As for triangles, there is a clear Richardson scaling range where the model results ($\langle I_1\rangle = 0.855$; $\langle I_2\rangle = 0.133$; $\langle I_3\rangle = 0.012$) are close to the DNS ($\langle I_1\rangle = 0.825$; $\langle I_2\rangle = 0.16$; $\langle I_3\rangle = 0.015$) and significantly different from the independent motion limit ($\langle I_1\rangle = 0.75$; $\langle I_2\rangle = 0.22$; $\langle I_3\rangle = 0.03$), although the differences from the DNS results are larger than for triangles. Again there is little difference between the diffusion equation and Thomson's model in the Richardson range. There are stronger differences at earlier times $t < t_0$, but this is to be expected since the diffusion model has no memory of the initial velocities whereas Thomson's model does. It is interesting that in the Richardson range, the model results correspond to slightly more extreme shapes (larger I_1 and smaller I_2 and I_3) than the DNS.

Tetrad shape factor PDFs are shown in Fig. 10 for Thomson's model. In contrast to the triangle results in Fig. 8, the initial evolution of the PDFs for I_1 and I_2 is not symmetrical, but is weighted

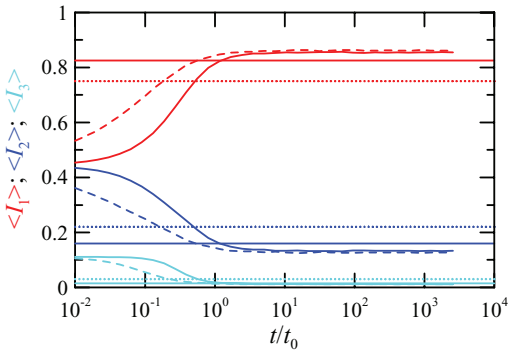

FIG. 9. Model estimates of the mean shape factors $\langle I_1\rangle$, $\langle I_2\rangle$, and $\langle I_3\rangle$ for initially right tetrahedra as a function of non-dimensional time for an initial separation $r_0/L = 10^{-9}$ and $C_0 = 7$, corresponding to $t_0/T_L = \frac{1}{2}C_0\,(r_0/L)^{2/3} = 3.5 \times 10^{-6}$. Red (top), blue (middle), and cyan (bottom) lines are for $\langle I_1\rangle$, $\langle I_2\rangle$, and $\langle I_3\rangle$, respectively. Solid curves are for Thomson's model and dashed curves are for the diffusion model. The solid horizontal lines are our DNS estimates in the inertial sub-range ($\langle I_1\rangle = 0.825$ and $\langle I_2\rangle = 0.16$ and $\langle I_3\rangle = 0.015$) and the dotted horizontal lines are the Monte Carlo independent motion estimates ($\langle I_1\rangle = 0.75$, $\langle I_2\rangle = 0.22$, and $\langle I_1\rangle = 0.03$).

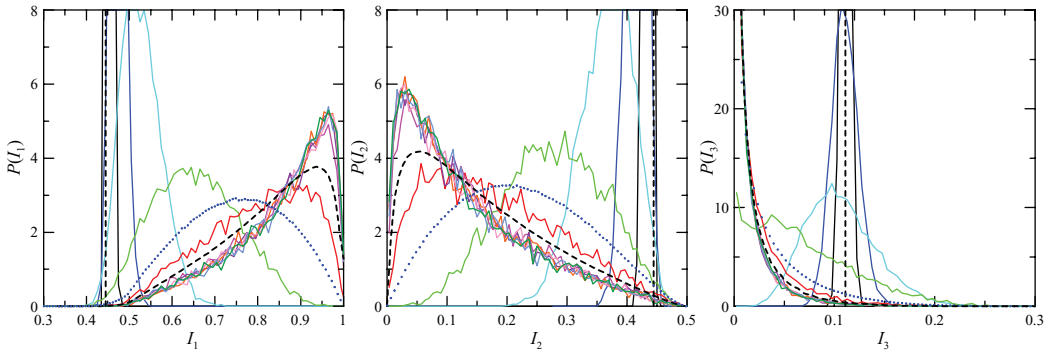

FIG. 10. Estimates of the PDFs for the shape factors I_1, I_2, and I_3 from Thomson's model for initially right tetrads for t/t_0 and r_0/L as in Fig. 8. The initial conditions are delta functions at $I_1 = I_2 = 4/9$ and $I_3 = 1/9$ as indicated by the vertical dashed lines. In each panel, the curves for $t/t_0 = 0.1, 0.3, \ldots, 8.1$ increase in width as the peak value moves further from the initial condition, and the remaining curves for $t/t_0 = 24.3, \ldots, 5.9 \times 10^3$ collapse to a self-similar form. The black dashed curve is the average over Richardson scaling times from DNS and the blue dotted curve is the independent motion diffusive limit.

towards more extreme shapes (larger I_1 and smaller I_2), and with increasing time the peak moves towards more extreme values. There is still a clear collapse to a similarity form in the Richardson range, but this is not achieved until $t/t_0 \approx 10$, and now we see some stronger departures from the DNS similarity results shown as the black dashed curve. We see that for both I_1 and I_2, the Richardson range similarity form of the PDF has a peak towards the high and low ends of the respective ranges, but for Thomson's model it is slightly more peaked than that for the DNS. This result is even stronger for the diffusion model (not shown). Still, the model results capture the main features of the departure from the independent motion limit which is shown as the dashed blue line. For I_3, the initial evolution of the PDF is more symmetrical and there is a collapse to a Richardson scaling form after $t/t_0 \approx 10$. In this case, the PDF strongly increases monotonically with decreasing I_3 and is in excellent agreement with the DNS results.

3. Trends with number of particles

Finally, we present some model results for clusters with $n > 4$. DNS calculations are yet to be done for these cases, but are planned. The mean shape factors shown in Fig. 11, particularly I_1 and I_2, converge rapidly with increasing n to values ≈0.82 and ≈0.15, respectively, for $n \approx 6$. For I_1 this is less than 20% smaller than the degenerate value of unity for $n = 2$, and only 4% smaller than its value for $n = 4$. As already noted in the analysis for $n \leq 4$, there is little difference between any of the models.

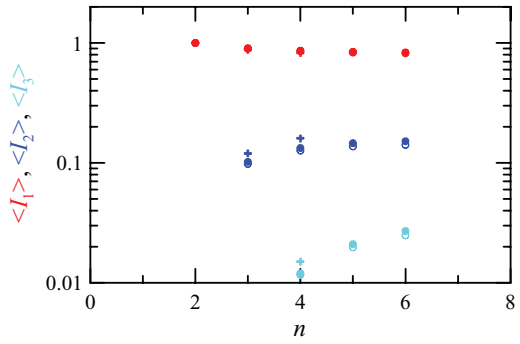

FIG. 11. Mean shape factors as a function of the cluster size n. DNS results for triangles and tetrads are shown as the + symbol, filled circles are for Thomson's model and open circles are for the diffusion model.

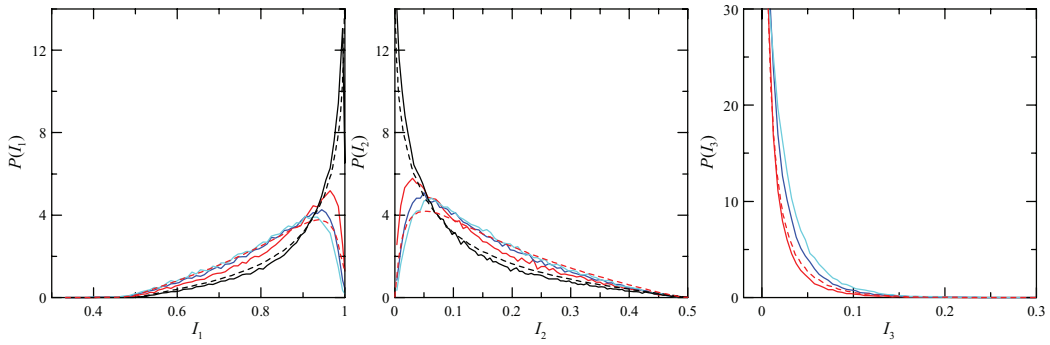

FIG. 12. Shape factor PDFs as a function of the cluster size n for Thomson's model (solid lines) and DNS (dashed lines). In the tails of the distributions, n increases from 3 to 6 from the lower to upper curves (black, red, blue, and cyan).

Figure 12 shows that PDFs for the three shape factors also converge for $n \approx 6$, and the limiting PDFs are less strongly peaked than those for smaller values of n. The only qualitative difference occurs with the addition of a third shape factor for $n > 3$. For $n = 3$, $P(I_1)$ and $P(I_2)$ have their peak values at $I_1 = 1$ and $I_2 = 0$ and decrease monotonically away from those values, while $P(I_3)$ is a delta function at the origin. These forms can be viewed as a relaxation away from the degenerate case $n = 2$ where the three PDFs are delta functions at $I_1 = 1$, $I_2 = 0$, and $I_3 = 0$, respectively. The introduction of a third non-zero shape factor for $n \geq 4$ ensures that $P(I_1)$ and $P(I_2)$ peak at $I_1 < 1$ and $I_2 > 0$ and the numerical results suggest that the PDFs vanish at $I_1 = 1$ and $I_2 = 0$, respectively. The monotonic form persists for $P(I_3)$ for all $n \geq 4$.

The main finding is that both the mean shape factors shown in Fig. 11 and the PDFs shown in Fig. 12 appear to converge with increasing n.

IV. CONCLUSIONS

We have shown that it is relatively straightforward to extend the"well-mixed" class of models to clusters of an arbitrary number n of particles whose motions are constrained by pair-wise spatial correlations; i.e., to Gaussian turbulence. This ignores both non-Gaussian and multi-point effects of the turbulence and so, by comparison with DNS results, enables us to examine the importance of those effects. In the class of well-mixed models we considered, the particle separation velocity has some "memory," so that the particle separation itself is non-Markovian. The memory is characterized by the Lagrangian time scale $2\sigma_u^2/C_0\langle\epsilon\rangle$ and in the limit of vanishing time-scale (i.e., $C_0 \to \infty$) all models approach a diffusion limit in which the separation is Markovian. For $n = 2$, this diffusion limit is essentially equivalent to Richardson's diffusion equation, and has analytical solutions for the mean-square dispersion and the separation PDF in the Richardson scaling range $t_0 \ll t \ll T_L$. This diffusion limit is also readily extended to $n > 2$.

Although the models of main interest to us here are non-diffusive (i.e., the separation is not Markovian), in all cases (all models we have studied and all $n \leq 6$) we find that in the Richardson scaling range the shape of the separation PDF is indistinguishable from that of Richardson's diffusion equation for $n = 2$. We conclude that matching the shape of Richardson's PDF is not a good test of whether relative dispersion is Markovian.

All the models (inevitably because of their construction) demonstrate a clear Richardson scaling regime for the mean-square separation and related quantities, and yield predictions for Richardson's constant g. With the Eulerian structure function fixed (at $C = 2$) the only parameter in the models is the Lagrangian structure function constant C_0 which controls the velocity memory. Thus, in the models g is a function of C_0 and, potentially, the number of particles n. Our main focus is on values of C_0 near the measured value of $C_0 \approx 7$ for DNS in forced isotropic turbulence. As with earlier studies, we find that for $n = 2$ different models give different values of g near or somewhat larger than the measured value $g \approx 0.5$. With increasing cluster size, we find that for a particular model (including the diffusion model) g increases exponentially. This is not a desirable property of the

models, since it implies that, for example, the scalar dissipation is a function of the cluster size. We believe that this strong dependence of g on n is an extension of the failure of these models to satisfy so-called "two-to-one" reduction. That is, in a hierarchy of one-, two-, . . . n-particle models, in general m-particle statistics calculated from m-particle and $(m + p)$-particle models ($p > 1$) are not equivalent. We illustrated this failure by looking at difference statistics and showing that the model prediction for the center-of-mass is increasingly in error with increasing n.

Despite these significant deficiencies regarding the mean-square separation, we find that the models do a much better job of predicting the shape of particle clusters. Both Thomson's model and the diffusion model give mean shape factors close to the DNS results for triangles and tetrads in the Richardson scaling range, and show significant deviations from the independent motion limit. Predicted shape factor PDFs are in very good agreement with DNS for triangles but show stronger differences for tetrads. In general, the models with memory give slightly better results than the diffusion model. The underlying physics seems to be that the pairwise spatial structure of the turbulence accounts for the major part of the difference from the independent motion limit, velocity memory gives a small improvement and non-Gaussian and multi-particle correlations account for the remainder.

Model results for the trends in shape factors with cluster size suggest convergence of both means and PDFs for $n \approx 6$.

From the point of view of practical modeling it has been suggested[26] that these models can be tuned to give the correct value of Richardson's constant simply by treating C_0 as an adjustable parameter. Our finding that the shape of the separation PDF is invariant for these models supports this approach, but the strong dependence of the Richardson constant on the number of particles in the cluster means that C_0 would need to be an increasing function of n. While this is feasible if the objective is to model the relative motion of multi-particle clusters, it is unlikely to be effective in modeling moments of the scalar field since then C_0 is also constrained by the single-particle dispersion in the far field which typically requires $C_0 \leq 7$.

ACKNOWLEDGMENTS

Direct numerical simulation data used for model comparisons in this paper were generated using advanced computing resources provided to the third author (P. K. Yeung) by the National Institute of Computational Sciences (at the University of Tennessee, USA) and the National Center for Computational Sciences (at Oak Ridge National Laboratory, USA). This work is also supported in part by NSF Grant No. CBET-1235906. This work was initiated while the first author (B. L. Sawford) was supported as a Visiting Professor by Cornell University.

[1] B. L. Sawford and J. F. Pinton, "A Lagrangian view of turbulent dispersion and mixing," in *Ten Chapters in Turbulence*, edited by P. A. Davidson, Y. Kaneda, and K. R. Sreenivasan (Cambridge University Press, Cambridge, 2013).
[2] C. W. Gardiner, *Handbook of Stochastic Methods for Physics, Chemistry and the Natural Sciences* (Springer, Berlin, 1983).
[3] A. S. Monin and A. M. Yaglom, *Statistical Fluid Mechanics* (MIT Press, Cambridge MA, 1975), Vol. 2.
[4] S. B. Pope, "Consistency conditions for random-walk models of turbulent dispersion," Phys. Fluids **30**, 2374 (1987).
[5] D. J. Thomson, "Criteria for the selection of stochastic models of particle trajectories in turbulent flows," J. Fluid Mech. **180**, 529 (1987).
[6] D. C. Haworth and S. B. Pope, "A generalized model for turbulent flows," Phys. Fluids **29**, 387 (1986).
[7] D. C. Haworth and S. B. Pope, "A pdf modelling study of self-similar turbulent free shear flows," Phys. Fluids **30**, 1026 (1987).
[8] D. J. Thomson and J. D. Wilson, "History of the Lagrangian stochastic model for turbulent dispersion," in *Lagrangian Modeling of the Atmosphere*, edited by A. K. Luhar (American Geophysical Union, Washington, 2012).
[9] S. B. Pope, "Simple models of turbulent flows," Phys. Fluids **23**, 011301 (2011).
[10] B. L. Sawford, "Turbulent relative dispersion," Annu. Rev. Fluid Mech. **33**, 289 (2001).
[11] J. P. L. C. Salazar and L. R. Collins, "Two-particle dispersion in isotropic turbulent flows," Annu. Rev. Fluid Mech. **41**, 405 (2009).
[12] D. J. Thomson, "A stochastic model for the motion of particle pairs in isotropic high-Reynolds-number turbulence, and its application to the problem of concentration variance," J. Fluid Mech. **210**, 113 (1990).
[13] M. S. Borgas and B. L. Sawford, "A family of stochastic models for two-particle dispersion in isotropic homogeneous stationary turbulence," J. Fluid Mech. **279**, 69 (1994).
[14] O. A. Kurbanmuradov, "Stochastic Lagrangian models for two-particle relative dispersion in high-Reynolds number turbulence," Monte Carlo Methods and Appl. **3**, 37 (1997).

[15] G. Pagnini, "Lagrangian stochastic models for turbulent relative dispersion based on particle pair rotation," J. Fluid Mech. **616**, 357 (2008).
[16] B. L. Sawford and P. K. Yeung, "Conditional relative acceleration statistics and relative dispersion modelling," Flow, Turbul. Combust. **85**, 345 (2010).
[17] B. Lüthi, J. Berg, S. Ott, and J. Mann, "Self-similar two-particle separation model," Phys. Fluids **19**, 045110 (2007).
[18] D. J. Thomson, "Diffusion of an instantaneous cluster of particles in homogeneous turbulence," Atmos. Environ., Part A **25**, 1725 (1991).
[19] L. F. Richardson, "Atmospheric diffusion shown on a distance neighbour graph," Proc. R. Soc. London, Ser. A **110**, 709 (1926).
[20] J. Berg, B. Lüthi, J. Mann, and S. Ott, "Backwards and forwards relative dispersion in turbulent flow: An experimental investigation," Phys. Rev. E **74**, 016304 (2006).
[21] T. Ishihara and Y. Kaneda, "Relative diffusion of a pair of fluid particles in the inertial subrange of turbulence," Phys. Fluids **14**, L69 (2002).
[22] B. L. Sawford, P. K. Yeung, and J. F. Hackl, "Reynolds number dependence of relative dispersion statistics in isotropic turbulence," Phys. Fluids **20**, 065111 (2008).
[23] J. F. Hackl, P. K. Yeung, and B. L. Sawford, "Multi-particle and tetrad statistics in numerical simulations of turbulent relative dispersion," Phys. Fluids **23**, 065103 (2011).
[24] H. Kaplan and N. Dinar, "A three dimensional stochastic model for concentration fluctuation statistics in isotropic homogeneous turbulence," J. Comput. Phys. **79**, 317 (1988).
[25] H. Kaplan and N. Dinar, "Comments on 'On the relative dispersion of two particles in homogeneous stationary turbulence and the implication for the size of concentration fluctuations at large times' by D. J. Thomson (1986, **112**, 890–894)," Q. J. R. Meteorol. Soc. **114**, 545 (1988).
[26] B. J. Devenish and D. J. Thomson, "A Lagrangian stochastic model for tetrad dispersion," J. Turbul. (in press).
[27] B. J. Devenish, "Geometrical properties of turbulent dispersion," Phys. Rev. Lett. **110**, 064504 (2013).
[28] B. Shraiman and E. Siggia, "Anomalous scaling for a passive scalar near the Batchelor limit," Phys. Rev. E **57**, 2965 (1998).
[29] G. K. Batchelor, *The Theory of Homogeneous Turbulence* (Cambridge University Press, Cambridge, 1953).
[30] P. A. Durbin, "A stochastic model of two-particle dispersion and concentration fluctuations in homogeneous turbulence," J. Fluid Mech. **100**, 279 (1980).
[31] P. K. Yeung and Y. Zhou, "Universality of the Kolmogorov constant in numerical simulations of turbulence," Phys. Rev. E **56**, 1746 (1997).
[32] M. S. Borgas and B. L. Sawford, "The small-scale structure of acceleration correlations and its role in the statistical theory of turbulent dispersion," J. Fluid Mech. **228**, 295 (1991).
[33] G. K. Batchelor, "The application of the similarity theory of turbulence to atmospheric diffusion," Q. J. R. Meteorol. Soc. **76**, 133 (1950).
[34] G. W. Stewart, "On the early history of the singular value decomposition," SIAM Rev. **35**, 551 (1993).
[35] P. Castiglione and A. Pumir, "Evolution of triangles in a two-dimensional turbulent flow," Phys. Rev. E **64**, 056303 (2001).
[36] A. Pumir, "Structure of the three-point correlation function of a passive scalar in the presence of a mean gradient," Phys. Rev. E **57**, 2914 (1998).
[37] M. S. Borgas and B. L. Sawford, "Molecular diffusion and viscous effects on concentration statistics in grid turbulence," J. Fluid Mech. **324**, 25 (1996).
[38] B. L. Sawford and P. K. Yeung, "Kolmogorov similarity scaling for one-particle Lagrangian statistics," Phys. Fluids **23**, 091704 (2011).